Direct observation of the hybridization gap in both the hidden order and large moment antiferromagnetic phases in URu_2Si_2

Wen Zhang,[1,2] Wei Feng,[1] Xuebing Luo,[1] Shiyong Tan,[1] Donghua Xie,[1] Yi Liu,[1] Yun Zhang,[1] Qunqing Hao,[1] Qiang Zhang,[1] Xiegang Zhu,[1] Qin Liu,[1,*] Qiuyun Chen,[1,†] and Xinchun Lai[1,‡]

[1]*Science and Technology on Surface Physics and Chemistry Laboratory, Mianyang, Sichuan 621908, People's Republic of China*

[2]*State Key Laboratory for Environment-Friendly Energy Materials, Southwest University of Science and Technology, Mianyang, Sichuan 621010, People's Republic of China*

(Received 8 June 2022; revised 20 September 2022; accepted 22 September 2022; published 10 October 2022)

Despite extensive research on the heavy fermion superconductor URu_2Si_2 in the past three decades, the nature of the hidden order (HO) phase transition occurring at 17.5 K remains ambiguous. Here we report a comparative scanning tunneling microscopy/spectroscopy (STM/STS) study on different terminations of the parent URu_2Si_2 and Fe-doped samples. A small gap, which was ascribed to the HO parameter by previous STM/STS studies, emerges in both the HO and large moment antiferromagnetic phases on the U terminations, indicating it is not the unique hallmark of the HO parameter. Moreover, a peak-gap-peak structure is observed on the Si terminations. Variations of the two spectral features with Fe concentration and temperature show that they stem from the alteration of f-c hybridization. The higher vanishing temperatures and larger sizes of the gap in the Fe-substituted samples indicate stronger f-c hybridization strength compared to URu_2Si_2. Our studies demonstrate hybridization is not the driving force for the HO phase transition.

DOI: 10.1103/PhysRevB.106.165109

I. INTRODUCTION

Since its first discovery in the 1980s [1], URu_2Si_2 has attracted substantial attention and has become one of the most important and enigmatic heavy fermion compounds due to its mysterious "hidden order (HO)" phase transition occurring at $T_0 \approx 17.5$ K as well as the unconventional superconductivity coexisting with the HO phase below $T_c \approx 1.5$ K [2,3]. Intriguingly, the HO phase transition in URu_2Si_2 was accompanied with a large entropy loss of $\Delta S \approx 0.2\,R\ln(2)$, which cannot be explained by the small antiferromagnetic moment of $(0.03 \pm 0.02)\ \mu_B$ per U atom detected by neutron-scattering experiments [4]. Enormous experimental efforts were dedicated to unveiling the nature of the order parameter below T_0, but in a sense no consensus has been reached [5–10].

On the one hand, density-wave state scenarios, such as charge density wave (CDW), spin density wave (SDW) [6], or chirality density wave [11], were proposed to be responsible for the HO phase transition in URu_2Si_2. On the other hand, a large body of experimental work found the evidence of band structure alterations during the HO phase transition [12–14]. It is noteworthy that scanning tunneling microscopy/spectroscopy (STM/STS) studies of URu_2Si_2 found a small partial particle-hole asymmetric energy gap emerges from the paramagnetic Kondo lattice state at a temperature very close to T_0 (within 1 K) in the dI/dV spectra [15,16]. STM-based quasiparticle interference (QPI) measurements revealed its origin as the splitting of a light band into two new heavy bands due to f-d hybridization [16], which leads to the deduction that HO phase transition is closely related to the hybridization process and this gap was identified as a hallmark of the hidden order parameter. However, later point contact spectroscopy (PCS) measurements found that the hybridization gap opens in the temperature range of 27–34 K, which is well above T_0, strongly implying that it is not the HO parameter [17].

There are many similarities between the HO and the large moment antiferromagnetic (LMAFM) phases in their transport, thermodynamic, and electronic properties in URu_2Si_2 [18,19]. The intimate relationship between the HO and LMAFM phases implies that their comparative studies may greatly promote our recognition of the HO parameter. Therefore, it is desirable and helpful to conduct comparative measurements of the two phases. The transition from HO to LMAFM phase occurs under appropriate pressures that range from 0.5 GPa at 0 K to 1.5 GPa at T_0 in URu_2Si_2 [20–22], which makes the effective electronic-structure study techniques such as STM or angle-resolved photoemission spectroscopy (ARPES) hard to reach. Fortunately, isoelectronic substitution of Ru with Fe in URu_2Si_2 can effectively act as chemical pressure and hence provides a precious opportunity to investigate both the HO and LMAFM phases under ambient pressure [23–27]. The temperature versus Fe concentration (T-x) phase diagram for $URu_{2-x}Fe_xSi_2$ has been well established and it can be equivalently converted to a T-P phase diagram [28]. Recent ARPES measurements found slight changes of the electronic structure between the LMAFM and HO phases, which suggests a close relationship between the hybridization and the HO [29]. In contrast,

*liuqin493@163.com
†chenqiuyun@caep.cn
‡laixinchun@caep.cn

PCS-based dI/dV measurements of P- and Fe-doped URu_2Si_2 revealed a hybridization gap in both the LMAFM and HO phases, indicating that hybridization is not the driving force of the HO phase transition [30]. Whether hybridization is the trigger for the HO phase transition is still under hot debate and further comparative investigations between the LMAFM and HO phases, i.e., Fe doped and the parent URu_2Si_2, may help to resolve the controversy.

In the present work, we report a comparative STM/STS study between the LMAFM and HO phases by using single crystals of the parent URu_2Si_2 and Fe-substituted $URu_{2-x}Fe_xSi_2$ with Fe concentrations $x = 0.15$ and 0.2. Statistical image observations find cleaving $URu_{2-x}Fe_xSi_2$ ($x = 0$, 0.15, and 0.2) single crystals results in two main types of unreconstructed terminations, i.e., U and Si terminations. STSs on the U terminations and Si terminations in URu_2Si_2 exhibit two different relatively broad asymmetric line shapes, which emerge at temperatures well above T_0 and can be well fitted by the single-impurity two-channel Fano formula with significantly different Fano line shape factors q. The fitting results suggest that these spectral features are induced by the Kondo screening of the local f moments with the conduction electrons, and the spectra on the U and Si terminations are dominated by tunneling into the light conduction electrons and the heavy f electrons, respectively. Remarkably, the gap structure on the U terminations and the peak-gap-peak structure on the Si terminations emerged at lower temperatures can also be clearly observed in $URu_{2-x}Fe_xSi_2$ ($x = 0.15$ and 0.2), which can be reasonably explained as the hybridization gap instead of the HO parameter.

II. METHODS

Single crystals of $URu_{2-x}Fe_xSi_2$ with three different Fe concentrations ($x = 0$, 0.15, and 0.2) were grown by the Czochralski method in a tetra-arc furnace under purified Ar gas and then subsequently annealed at 900 °C under ultrahigh vacuum for 10 days. The quality of the grown single-crystal samples was determined with x-ray powder diffraction (XRD) measurements with a commercial x-ray diffractometer using Cu $K\alpha$ radiation (see Fig. S1 in the Supplemental Material) [31].

Electrical transport measurements were conducted by using a commercial Physical Property Measurement System (see Fig. S2 in the Supplemental Material) [31]. All the STM measurements were performed by utilizing a commercial low-temperature STM apparatus installed in an ultrahigh-vacuum chamber with a base pressure greater than 2.0×10^{-11} mbar. Clean tungsten tips were used after Ar^+ sputtering and after being treated on a clean Cu (111) surface before performing the measurements on the $URu_{2-x}Fe_xSi_2$ samples. The tunneling differential conductance (dI/dV) spectra were recorded by a standard lock-in technique with a modulation amplitude of 1 mV.

III. EXPERIMENTAL RESULTS

A. Identification of different terminated surfaces

Single crystals of $URu_{2-x}Fe_xSi_2$ ($x = 0$, 0.15, and 0.2) were cleaved perpendicular to the c axis in the ultrahigh-vacuum chamber to obtain clean surfaces before STM measurements. Based on substantial STM observations after dozens of experiments, we find the cleavages produce three types of terminations with apparently different surface topographies, which are denoted as surfaces A − C in Figs. 1(a)–1(c), respectively. The measured height profiles [see Fig. 1(a)] show that surface A usually lies 1.1 Å above or 3.8 Å below surface B. It is easy to obtain the atomically resolved topographic image on surface A as shown in Fig. 1(b). whereas the topographic images of surfaces B [Figs. 1(a) and 1(c)] usually exhibit some dimmed patterns with various shapes and sizes at the same tunneling set point ($V_b = 20$ mV, $I = 60$ pA). Via further reducing the tip-sample distance by using a small tunneling junction resistance of 0.5 MΩ ($V_b = 1$ mV, $I = 2$ nA) during imaging, the atomic structure of surface B was acquired and shown in the inset of Fig. 1(a). Surfaces A and B display the same tetragonal lattice structure with an atomic spacing of 4.2 Å. In view of the bulk lattice structure of URu_2Si_2 in Fig. 1(g), these two types of surfaces should be U or Si layers, which show the same atomic structure with a theoretical nearest-neighbor distance of 4.13 Å. Furthermore, according to the measured step height between two neighboring terraces [Fig. 1(c)], surface B can be determined as the Si-terminated layer because the 2.2 Å step height just equal to the spacing between two neighboring Si layers, whereas the spacing between two neighboring U layers is 4.8 Å, which is much larger than the measured 2.2 Å step height. As a consequence, surface A should be the U-terminated layer. Ultimately, since the 2.4 Å relative height between surfaces C and A [see Fig. 1(b)] agrees well with the interplanar spacing between the Ru and U layers in the URu_2Si_2 crystal structure, surface C is ascribed to the Ru-terminated layer. In addition, the Ru-terminated surfaces exhibit a (2×2) reconstruction, the atomic arrangement of which is rotated by 45 ° relative to those on the Si or U layers. Figs. 1(d)–1(f) show the typical dI/dV spectra detected on the U-, Si-, and Ru-terminated surfaces, respectively, and the primary spectral features of the U and Si terminations accord with those reported by Aynajian *et al.* [15].

B. Comparison of electronic properties between the HO and LMAFM phases

After successful identification of surfaces A − C, we then systematically compared the electronic properties of the parent URu_2Si_2 with those of two Fe-substituted samples on two unreconstructed terminations, i.e., U and Si layers. Figures 2(a)–2(c) show the atomically resolved topographic images of the U-terminated surfaces of URu_2Si_2, $URu_{1.85}Fe_{0.15}Si_2$, and $URu_{1.8}Fe_{0.2}Si_2$, respectively. For URu_2Si_2, the U surface displays well-ordered tetragonal lattice structure with equal height contrast of all the uranium atoms. In contrast, the surface atoms on the U terminations of $URu_{1.85}Fe_{0.15}Si_2$ and $URu_{1.8}Fe_{0.2}Si_2$ show inhomogeneous height contrast and there are defects induced by Fe doping randomly distributing on the surface. In order to check whether the dimmer or brighter area will affect the spectral features, we collected dI/dV spectra above a series of sites marked by the white dots in the topographic images [Figs. 2(a)–2(c)] and displayed them in Figs. 2(d)–2(f).

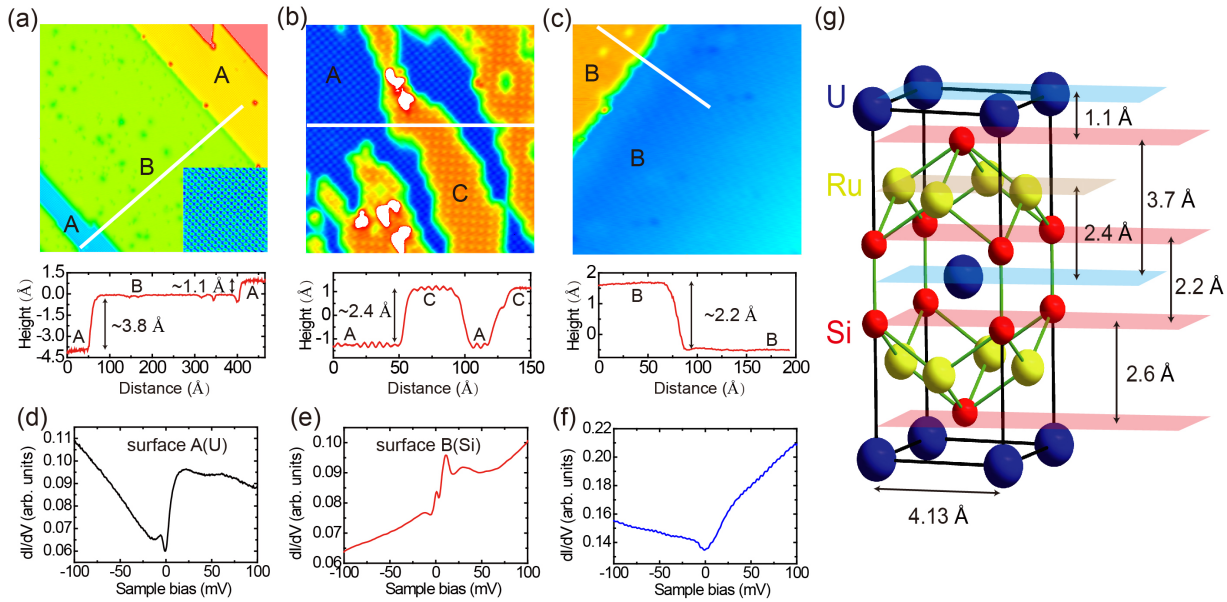

FIG. 1. STM topographies of the cleaved URu_2Si_2 single-crystal and typical tunneling differential conductance (dI/dV) spectra taken on three different types of terminated surfaces (termed as surfaces A−C) at 4.5 K. (a) Topographic image showing the relative heights between surfaces A and B ($V_b = 20$ mV, $I = 60$ pA, $50 \times 50\,\mathrm{nm}^2$). (b) Topographic image showing the relative heights between surfaces A and C ($V_b = 20$ mV, $I = 60$ pA, $15 \times 15\,\mathrm{nm}^2$). (c) Topographic image showing the relative heights between two neighboring surfaces B ($V_b = 20$ mV, $I = 60$ pA, $30 \times 30\,\mathrm{nm}^2$). The height profiles measured along the white lines in the topographic images (a)–(c) are shown at the bottom of each panel. The inset in panel (a) shows the atomically resolved topographic image of surface B ($V_b = 1$ mV, $I = 2$ nA, $7 \times 7\,\mathrm{nm}^2$). (d)–(f) Spatially averaged dI/dV spectra detected on surfaces A–C, respectively. (g) Schematic diagram illustrating the layered structure of URu_2Si_2 and the interplanar spacing between different atomic layers.

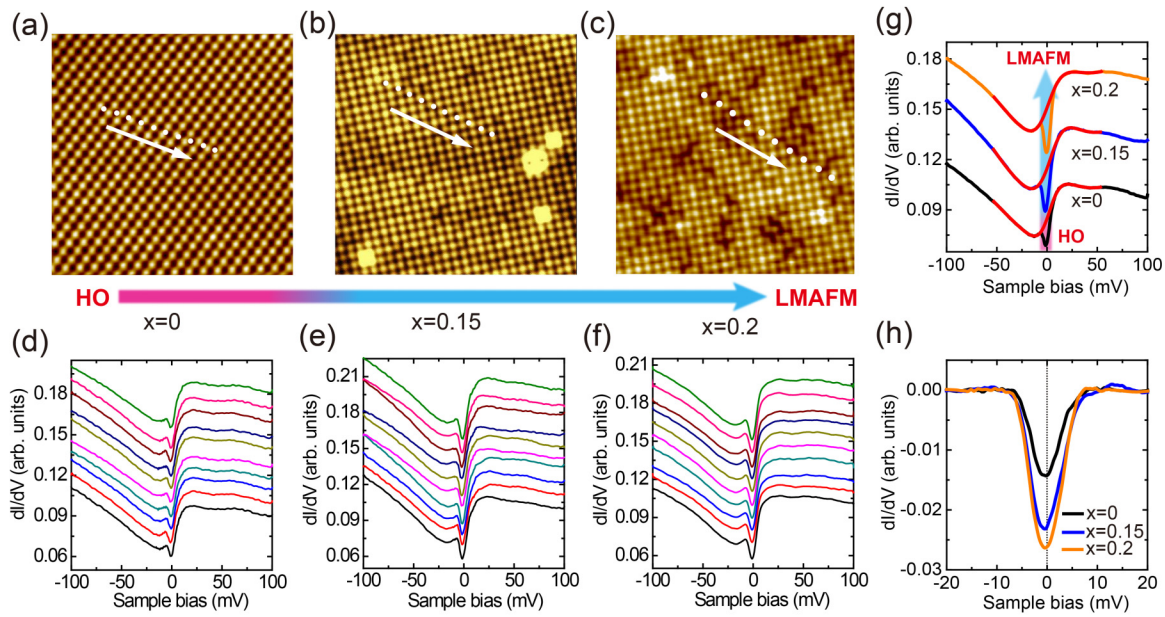

FIG. 2. Comparison of the tunneling differential conductance spectra taken on the U terminations of $URu_{2-x}Fe_xSi_2$ with different Fe concentrations. (a)–(c) Topographic images on the U-terminated surfaces of $URu_{2-x}Fe_xSi_2$ with Fe concentration $x = 0$, 0.15, and 0.2 ($V_b = 20$ mV, $I = 60$ pA, $10 \times 10\,\mathrm{nm}^2$). (d)–(f) A series of dI/dV spectra taken at the positions marked by the white dots in panels (a)–(c), respectively. The direction from bottom to top in panels (d)–(f) corresponds to the direction indicated by the white arrow in panels (a)–(c), respectively. (g) Spatially averaged spectra detected on the U-terminated surfaces of $URu_{2-x}Fe_xSi_2$ with $x = 0$, 0.15, and 0.2. The red lines are the fits by the Fano line shape, excluding the data points in the range of −7 to 7 mV. The spectra in each panel [from (d) to (g)] are shifted vertically for clarity. (h) Direct comparison of the dI/dV spectra shown in panel (g) after subtracting their corresponding Fano fits. All the measurements were performed at 4.5 K.

TABLE I. Fitted Fano parameters of the dI/dV spectra on the U-terminated surfaces.

Parameters	URu_2Si_2	$URu_{1.85}Fe_{0.15}Si_2$	$URu_{1.8}Fe_{0.2}Si_2$
Q	1.00	1.23	0.98
E_0/mV	2.35	4.66	0.45
Γ/mV	18.01 ± 0.04	22.12 ± 0.09	22.39 ± 0.06

Although the intensities of the dI/dV signal change slightly with the positions on the U surfaces of $URu_{1.85}Fe_{0.15}Si_2$ and $URu_{1.8}Fe_{0.2}Si_2$, the major features remain unchanged. In addition, we have randomly detected the topographic images and dI/dV spectra in different regions of the same samples and also on different samples (see Figs. S3 and S4 in the Supplemental Material) [31]. These spectra in Fig. S3 or Fig. S4 are nearly the same as each other and exhibit the same features as those shown in Fig. 2(e) or 2(f), respectively [31]. In order to thoroughly eliminate the effect of measuring positions and acquire the general nature of different Fe-doped samples, we averaged dozens of dI/dV spectra taken at various sites on the U-terminated surfaces before comparing their properties. Surprisingly, the spatially averaged spectra on the two Fe-substituted samples [Fig. 2(g)] show two features similar to that on the parent URu_2Si_2, including a small particle-hole asymmetric gap around E_F and a relatively wider asymmetric line shape background. The emergence of the gap structure around E_F, which was ascribed to the spectroscopic signature of the hidden order parameter of URu_2Si_2 in the previously reported STM studies [15,16], is quite unexpected here, since these Fe-substituted samples are completely in the LMAFM phase at the measured temperature of 4.5 K [32]. The emergence of the so-called HO gap in the LMAFM phase implies that this gap is not a unique signature of the hidden order parameter. For the wider asymmetric line shape, it is generally regarded as the signature of the Kondo resonance [33]. Previous STM studies presented the evolution of this spectral feature from 120 to 20 K [15], and the results are well in line with the single Kondo impurity model. Indeed, after processing the data by excluding the small gap structure, the dI/dV spectra of both the unsubstituted and Fe-substituted samples taken at 4.5 K can be well described by the two-channel Fano formula [see red curves in Fig. 2(g)]:

$$\frac{dI}{dV} \equiv g(V) \propto \frac{(q+\varepsilon)^2}{\varepsilon^2+1}, \quad \varepsilon = \frac{V-E_0}{\Gamma}, \tag{1}$$

where ε_0 is the energy position of the Kondo resonance state relative to E_F, Γ is the half width at half maximum of the resonance curve and is proportional to the hybridization strength between the localized f states and itinerant states, and q is the line shape parameter [15,16,33,34]. The fitting parameters are shown in Table I. It is noteworthy that the values of Γ of $URu_{1.85}Fe_{0.15}Si_2$ and $URu_{1.8}Fe_{0.2}Si_2$ are larger than that of URu_2Si_2, implying an enhancement of the hybridization strength between U-5f electrons and itinerant electrons with Fe substitution. In a recent transport study combined with tight-binding calculations, isoelectronic substitution of Fe or Os for Ru in URu_2Si_2 was also found to increase the f-d hybridization [35], which is in good agreement with our results.

In order to solely extract the change of the small gap with Fe substitution, the Fano line shape background was subtracted from the measured data as shown in Fig. 2(h). Remarkably, both the depth and width of this gap increase with Fe concentration in $URu_{2-x}Fe_xSi_2$. Previous STM-based QPI measurements clearly revealed the splitting of a light band into two heavier bands within an energy range coincident with the small gap and provided strong evidence that this gap is induced by the alteration of the f-d hybridization process [16]. PCS-based dI/dV spectra also detected the opening of a hybridization gap in the HO and LMAFM phases of $URu_{2-x}Fe_xSi_2$ ($x = 0, 0.02, 0.07, 0.17$) [30], which is consistent with the overall trend of our observations. Based on the above points, it is quite reasonable to speculate that the small gap stems from the alteration of the hybridization process, instead of the HO phase transition. This conclusion is a natural and rational result, since a conventional hybridization interaction occurs as a crossover process and induces band renormalization, which does not involve any symmetry breaking and should not cause a second-order phase transition.

For comparison, the results on the Si terminations of $URu_{2-x}Fe_xSi_2$ ($x = 0$, 0.15, and 0.2) are shown in Fig. 3. Dimmed holes with various sizes appear on the Si terminations of all three samples. In order to find whether these dimmed holes will affect the spectroscopic features, we measured a series of dI/dV spectra across them. As shown in Figs. 3(d)–3(f), the major spectral features are not altered by the presence of those dimmed patterns, which is also demonstrated by the dI/dV spectra taken on different regions of the same samples and also on different samples (see Figs. S5 and S6 in the Supplemental Material) [31]. Then the spectra taken at various locations of the Si terminations were averaged to thoroughly eliminate the influence of measuring positions. The spatially averaged spectra on the Si terminations of the three samples in Fig. 3(g) show similar features: a gap around E_F accompanied by two peaks on its left and right sides and a wider asymmetric line shape background. The asymmetric line shape background can also be well fitted by the Fano spectrum [Eq. (1)] after excluding the detailed structures around E_F, i.e., the small gap and lower peak, as shown by the red curves in Fig. 3(g). The Fano fits on the Si terminations for all three crystals yield much larger q values than those on the U terminations (see Table II). The value of q determines the line shape of the spectrum and generally produces a Lorentzian peak, a Lorentzian dip, and an asymmetric line shape as q, respectively, approaches infinity, 0, and 1, which essentially reflects the relative strength between indirect tunneling into the Kondo resonance state and direct tunneling into the itinerant states. The much larger q values on the Si termination imply that electrons more readily tunnel into the Kondo-screened U-5f electrons instead of the itinerant conduction electrons; even the measured top atomic layer is full of Si atoms. Previous STM/STS studies mapped out the spatial dependence of Fano fitting parameters on the U-terminated surfaces of URu_2Si_2 with atomic resolution and found that the maximum q values occur at the fourfold hollow sites instead of atop the U atoms [15]. An analogous phenomenon was also discovered in the famous lanthanide-based 4f heavy fermion system $CeCoIn_5$, in which the strength of tunneling into the heavy 4f states is more pronounced on the Co layers

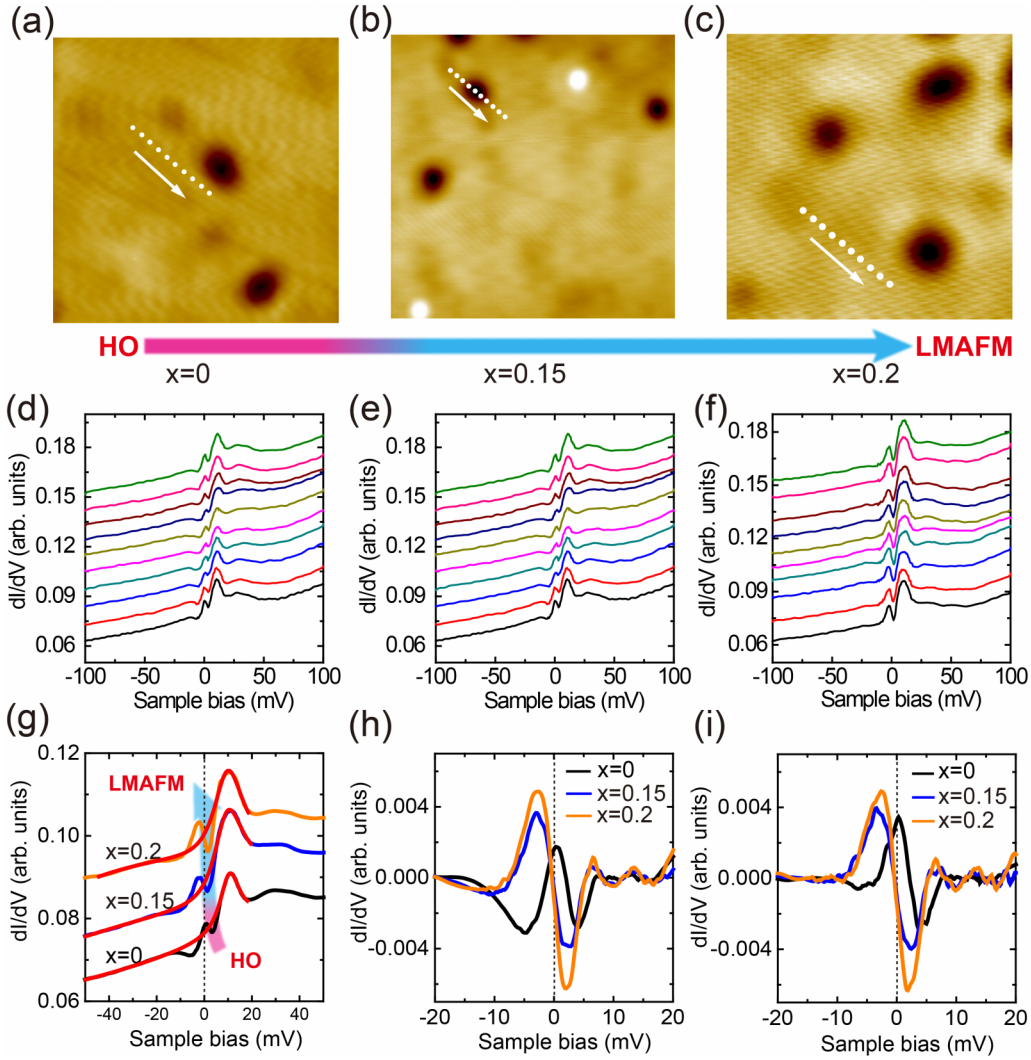

FIG. 3. Comparison of the tunneling differential conductance spectra taken on the Si terminations of $URu_{2-x}Fe_xSi_2$ with different Fe concentrations. (a)–(c) Topographic images taken on the Si-terminated surfaces of $URu_{2-x}Fe_xSi_2$ with Fe concentration $x = 0$, 0.15, and 0.2 ($V_b = 20$ mV, $I = 60$ pA, $10 \times 10\,\mathrm{nm}^2$). (d)–(f) A series of dI/dV spectra taken above the positions marked by white dots in panels (a)–c), respectively. The direction from bottom to top in panels (d)–(f) corresponds to the direction indicated by the white arrow in panels (a)–(c), respectively. (g) Spatially averaged spectrum detected on the Si-terminated surfaces of $URu_{2-x}Fe_xSi_2$ with $x = 0$, 0.15, and 0.2. The red lines are the fits by the Fano line shape, excluding the data points in the range of –10 to 10 mV. The spectra in each panel [from (d) to (g)] are shifted vertically for clarity. (h) Direct comparison of the dI/dV spectra shown in panel (g) after subtracting their corresponding Fano fits. (i) The same spectra from panel (h) after subtracting the data measured at 20 K. All the topographic images and primitive dI/dV spectra were taken at 4.5 K.

instead of on the Ce-In layers [36]. These experimental observations indicate that the orientation of atomic orbitals, as well as the selective hybridization among different suborbitals, is also crucial for the tunneling process. The stronger coupling to heavier f excitations on the Si layers observed here is probably due to the larger amplitude of hybridization of f states with the out of plane spd electrons than that with the in-plane spd electrons, which is similar to the case revealed by the first-principle calculations for $CeIrIn_5$ [37]. In addition, for the Si terminations, the values of Γ in the Fe-substituted crystals also increase by half as compared with the one in the parent URu_2Si_2, resembling the results detected on the U terminations and further confirming a stronger hybridization strength in the Fe-substituted crystals.

TABLE II. Fitted Fano parameters of the dI/dV spectra on the Si-terminated surfaces.

Parameters	URu_2Si_2	$URu_{1.85}Fe_{0.15}Si_2$	$URu_{1.8}Fe_{0.2}Si_2$
q	12.86	4.51	6.40
E_0/mV	10.34	8.72	9.05
Γ/mV	5.17 ± 0.04	7.45 ± 0.11	7.73 ± 0.20

After successively subtracting the Fano fits and spectra taken at 20 K from the measured data, the remaining spectra all exhibit an asymmetric peak-gap-peak structure as shown in Figs. 3(h) and 3(i). The amplitude of the peak-gap-peak feature increases with Fe concentration in $URu_{2-x}Fe_xSi_2$ and their energy positions in the two Fe-substituted crystals are

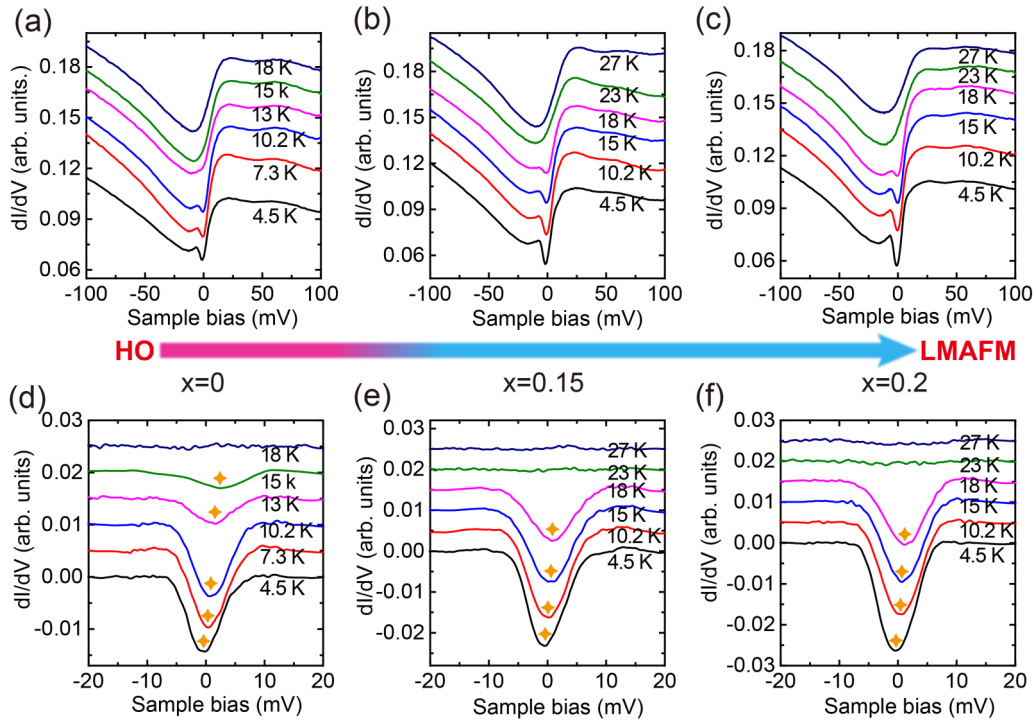

FIG. 4. Temperature dependence of the dI/dV spectra on the U terminations of $URu_{2-x}Fe_xSi_2$ with different Fe concentrations. (a)–(c) A series of spatially averaged dI/dV spectra taken at various temperatures on the U-terminated surfaces of $URu_{2-x}Fe_xSi_2$ with $x = 0$, 0.15, and 0.2, respectively. (d)–(f) Comparison of the temperature evolution of the small gap around E_F detected on the U-terminated surfaces of $URu_{2-x}Fe_xSi_2$ with $x = 0$, 0.15, and 0.2. The spectra in panels (d)–(f) are derived from those in panels (a)–(c) by subtracting their Fano fits. Spectra in each panel are shifted vertically for clarity.

discernibly shifted towards lower energy by about 2 mV as compared with that in the parent URu_2Si_2. The increasing spectral feature's amplitude with Fe doping is reminiscent of a similar variation of the small gap on the U terminations [Fig. 2(h)], which thus reflects the enhanced f-c hybridization in the Fe-substituted samples. Meanwhile, the shifting behavior may also be induced by the increased hybridization strength, since similar shifting behavior of the electron pockets originating from the enhanced hybridization due to Fe doping was also observed in a recent ARPES study on $URu_{2-x}Fe_xSi_2$ ($x = 0$, 0.2) [29]. Consequently, this peak-gap-peak structure on the Si terminations also arises from the alteration of the f-c hybridization.

C. Temperature evolution of the dI/dV spectra in the HO and LMAFM phases

Comparative study of the temperature evolution of the tunneling spectra on the U and Si terminations in pristine URu_2Si_2 and Fe-substituted samples $URu_{2-x}Fe_xSi_2$ ($x =$ 0.15, 0.2) are shown in Figs. 4 and 5. On the U-terminated surfaces (Fig. 4), the small gap near E_F is gradually suppressed with increasing temperature in all three compounds, and it completely disappears at 18 K in the parent URu_2Si_2. Noticeably, this gap feature is clearly visible at 18 K in $URu_{1.85}Fe_{0.15}Si_2$ [Figs. 4(b) and 4(e)] and $URu_{1.8}Fe_{0.2}Si_2$ [Figs. 4(c) and 4(f)] and vanishes at a much higher temperature of 23 K. The vanishing temperature of the gap structure in the Fe-doped samples is very close to the transition temperature from PM to LMAFM phase in $URu_{1.85}Fe_{0.15}Si_2$ (23.5 K), but different from that in $URu_{1.8}Fe_{0.2}Si_2$ (28.5 K) (see Fig. S2) [31]. This further supports that the emergence of the small gap in $URu_{2-x}Fe_xSi_2$ ($x = 0$, 0.15, 0.2) is related to the f-c hybridization instead of the PM-HO or PM-LMAFM phase transitions. The higher vanishing temperatures in the two Fe-substituted samples also indicate stronger f-c hybridization strength compared to the parent URu_2Si_2. Moreover, as shown in Figs. 4(d)–4(f), the position of this gap slightly shifts towards higher energies with increasing temperature in all three crystals, which shows good consistence with the shifting of the peak-gap-peak feature with Fe concentration on the Si terminations [Figs. 3(h) and 3(i)]. Similar shifting behaviors have also been observed in the previous STM studies [15,16].

On the Si terminations, the gap and lower peak are gradually smeared out upon increasing temperature and the spectra ultimately evolve into a single-peak structure in all three samples as revealed in Figs. 5(a)–5(c). As shown in Figs. 5(d)–5(f), for URu_2Si_2, the remaining peak-gap-peak spectral feature after subtracting the broad Fano line shape is completely indiscernible at 16 K, whereas for $URu_{1.85}Fe_{0.15}Si_2$ or $URu_{1.8}Fe_{0.2}Si_2$, this feature is distinctly visible at 16 K and vanishes at 20 K. Obviously, for the Si terminations, the onset temperature of the peak-gap-peak feature in the parent URu_2Si_2 is lower than those in the Fe-substituted crystals, which agrees well with the tendency observed on the U terminations and again indicates an enhanced hybridization in the Fe-doped samples. Besides, the onset temperatures of the peak-gap-peak feature in all three compounds are overall lower than the bulk PM-HO or PM-LMAFM phase transition temperatures determined from electrical transport

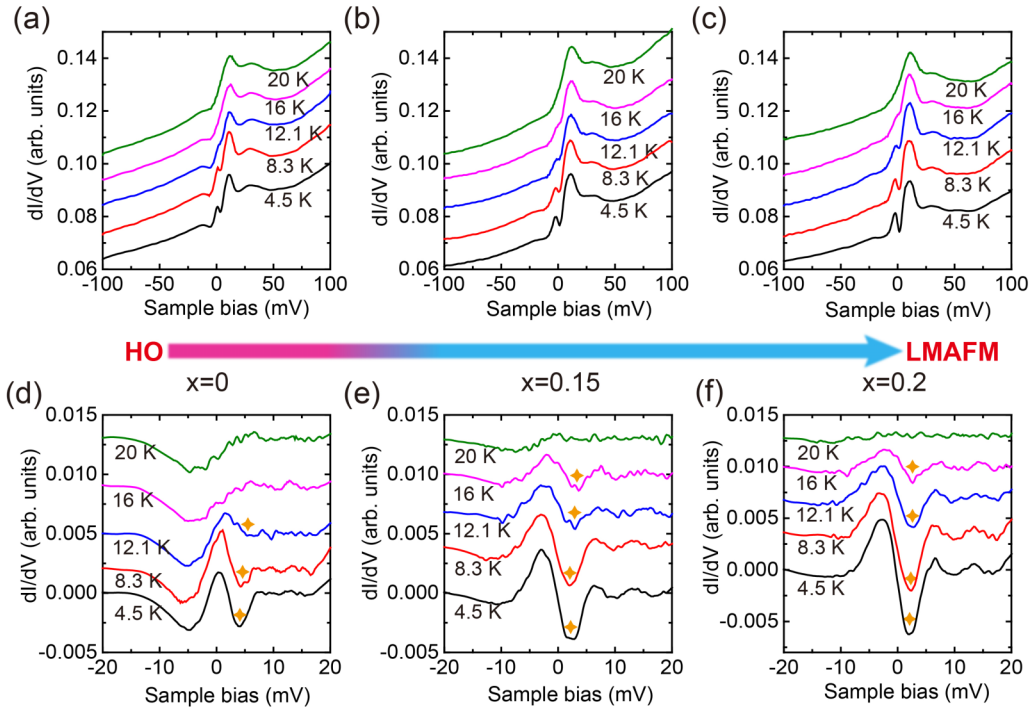

FIG. 5. Temperature dependence of the dI/dV spectra on the Si terminations of $URu_{2-x}Fe_xSi_2$ with different Fe concentrations. (a)–(c) A series of spatially averaged dI/dV spectra taken at various temperatures on the Si-terminated surfaces of $URu_{2-x}Fe_xSi_2$ with $x = 0$, 0.15, and 0.2, respectively. (d)–(f) Spectra derived by subtracting the Fano fits from those experimental data shown in panels (a)–(c). Spectra in each panel are shifted vertically for clarity.

measurements (see Fig. S2) [31] or the opening temperatures of the small gap on the U terminations. The former excludes the association between the emergence of the peak-gap-peak feature and the PM-HO or PM-LMAFM phase transitions. The cause of the latter will be discussed later.

IV. DISCUSSION

The peak-gap-peak structure on the Si terminations is highly similar to the hybridization gap detected by PCSs [30] and it also tallies with the characteristic spectroscopic structure (i.e., a gap surrounded by two asymmetric peaks) of the Kondo lattice predicted by a theoretical model, which considers the periodic Anderson hybridization picture plus quantum interference between two channels [38]. Thus, we deem that this peak-gap-peak structure, which arises from the alteration of the f-c hybridization, presumably signifies the full development of Kondo coherence. Moreover, we suspect that the small gap on the U terminations and the peak-gap-peak structure on the Si terminations, respectively, represents the spectral structure sensitive to the direct hybridization gap with strong coupling to the light electrons and the indirect hybridization gap with strong coupling to the f electrons, since their sizes and line shapes highly resemble the theoretically predicted spectral structure dominated by the direct and indirect gap produced by the hybridization-modified renormalized band structures in the Kondo lattice. The lower onset temperatures of the peak-gap-peak feature on the Si terminations compared to the opening temperatures of the small gap on the U terminations in all three compounds meet our expectation, since the width of the indirect hybridization gap on the Si terminations is narrower than that of the direct hybridization gap on the U terminations, and the former is easier to smear out by thermal broadening than the latter upon increasing temperature. This deduction also shows good consistency with the much larger q values on the Si terminations than on the U terminations acquired from the single-impurity Fano fits (Tables I and II). Similarly, in the $4f$−based heavy fermion system $CeCoIn_5$, the double-peak structure on the Co layers, representing the indirect hybridization gap, evolves into a single peak around 50 K, whereas the direct hybridization gap on the Ce-In layers closes at a much higher temperature [36].

Notably, the development of the Kondo coherence in a heavy fermion system usually occurs as a crossover process and thus the accurate definition of the onset temperature for complete formation of the Kondo coherence is to some extent controversial. Different experimental techniques usually yield different coherence temperatures for the same compound. Conventional coherence temperature T^* is defined as the maximum point in the ρ-T curve. Yet, in many famous heavy fermion materials, T^*, detected by the transport measurements, is usually different from the coherence temperature directly determined by the alterations of the electronic structures measured by ARPES [39]. For URu_2Si_2, PCS studies established that Kondo coherence temperatures are in the range of 27–34 K [17], while the resistivity maximum temperature T^* is around 70–80 K and the rounded maximum in the susceptibility-temperature curve is at 55 K [1,6]. In the meantime, some ARPES studies find the formation of a coherent heavy fermion liquid across the HO phase transition [13], while others observe that a hybridization gap of about 11 meV opens at $T > T_0$ [12]. In our STS measurements,

the onset temperatures of the direct or indirect hybridization gap are smaller than T^* and the coherence temperatures determined by QPS techniques in both the parent URu_2Si_2 and Fe-doped crystals. One possible reason may account for this discrepancy. Since STM is a highly surface-sensitive technique, surface effects may be responsible for the reduced coherence temperatures. The decreased U coordination number on the surface may result in the decreased hybridization, leading to a considerably lower Kondo coherence temperature, as observed in the Ce-based systems [39].

V. CONCLUSIONS

In conclusion, our comparative STM/STS studies on parent URu_2Si_2 and Fe-substituted $URu_{2-x}Fe_xSi_2$ ($x = 0.15, 0.2$) reveal that a small gap feature on the U terminations, which was once ascribed to the hidden order parameter by previous STS studies, exists in both the HO and LMAFM phases and it actually stems from the hybridization between f electrons and itinerant states. The hybridization gradually reveals itself by two stages in the measured STSs: relatively broader asymmetric Fano line shapes, which follow the single-impurity Kondo resonance behavior and begin at temperatures well above T_0, and narrower spectral structures around E_F, signifying the formation of coherence in the Kondo lattice at lower temperatures. The hybridization-modified STSs on both Si and U terminations display notably different detailed structures due to the different predominant tunneling ratio among the two channels in the quantum-interference tunneling process. On the Si terminations, the tunneling spectra show strong coupling to the f components, embodied by a large q factor in the Fano fitting for the broader asymmetric line shape and a characteristic indirect hybridization gap feature of the Kondo lattice, i.e., a peak-gap-peak structure, at lower temperatures. However, on the U terminations, the spectra show strong coupling to the light itinerant components, reflected by a small q value in the Fano fitting and a direct hybridization gap feature. Moreover, all these hybridization-related spectral features exist in both the parent URu_2Si_2 and Fe-substituted $URu_{2-x}Fe_xSi_2$, and the hybridization strength is relatively stronger in the Fe-doped samples at the same temperature. Our STM/STS results provide an important clue to unravel the origin of the HO phase transition by demonstrating that hybridization is not the driving force for the HO phase transition.

ACKNOWLEDGMENTS

This work was supported by the National Natural Science Foundation of China (Grants No. 12122409, No. 11874330, No. 11904335, No. 11904334, and No. 12004349), the National Key Research and Development Program of China (Grants No. 2021YFA1601100, No. 2017YFA0303104, and No. 2016YFA0300200), and the Natural Science Foundation of the Southwest University of Science and Technology (Grant No. 19zx7127).

[1] T. T. Palstra, A. A. Menovsky, J. van den Berg, A. J. Dirkmaat, P. H. Kes, G. J. Nieuwenhuys, and J. A. Mydosh, Superconducting and Magnetic Transitions in the Heavy-Fermion System URu_2Si_2, Phys. Rev. Lett. **55**, 2727 (1985).

[2] J. A. Mydosh and P. M. Oppeneer, Colloquium: Hidden order, superconductivity, and magnetism: The unsolved case of URu_2Si_2, Rev. Mod. Phys. **83**, 1301 (2011).

[3] J. A. Mydosh and P. M. Oppeneer, Hidden order behaviour in URu_2Si_2 (a critical review of the status of hidden order in 2014), Philos. Mag. **94**, 3642 (2014).

[4] C. Broholm, J. K. Kjems, W. J. Buyers, P. Matthews, T. T. Palstra, A. A. Menovsky, and J. A. Mydosh, Magnetic Excitations and Ordering in the Heavy-Electron Superconductor URu_2Si_2, Phys. Rev. Lett. **58**, 1467 (1987).

[5] J. A. Mydosh, P. M. Oppeneer, and P. S. Riseborough, Hidden order and beyond: An experimental-theoretical overview of the multifaceted behavior of URu_2Si_2, J. Phys.: Condens. Matter **32**, 143002 (2020).

[6] M. B. Maple, J. W. Chen, Y. Dalichaouch, T. Kohara, C. Rossel, M. S. Torikachvili, M. W. McElfresh, and J. D. Thompson, Partially Gapped Fermi Surface in the Heavy-Electron Superconductor URu_2Si_2, Phys. Rev. Lett. **56**, 185 (1986).

[7] A. F. Santander-Syro, M. Klein, F. L. Boariu, A. Nuber, P. Lejay, and F. Reinert, Fermi-surface instability at the 'hidden-order' transition of URu_2Si_2, Nat. Phys. **5**, 637 (2009).

[8] R. Yoshida, Y. Nakamura, M. Fukui, Y. Haga, E. Yamamoto, Y. Ōnuki, M. Okawa, S. Shin, M. Hirai, Y. Muraoka *et al.*, Signature of hidden order and evidence for periodicity modification in URu_2Si_2, Phys. Rev. B **82**, 205108 (2010).

[9] J. S. Hall and T. Timusk, Optical study of hybridization and hidden order in URu_2Si_2, Philos. Mag. **94**, 3760 (2014).

[10] C. R. Wiebe, J. A. Janik, G. J. MacDougall, G. M. Luke, J. D. Garrett, H. D. Zhou, Y. J. Jo, L. Balicas, Y. Qiu, J. R. D. Copley *et al.*, Gapped itinerant spin excitations account for missing entropy in the hidden-order state of URu_2Si_2, Nat. Phys. **3**, 96 (2007).

[11] H. H. Kung, R. E. Baumbach, E. D. Bauer, V. K. Thorsmølle, W. L. Zhang, K. Haule, J. A. Mydosh, and G. Blumberg, Chirality density wave of the "hidden order" phase in URu_2Si_2, Science **347**, 1339 (2015).

[12] F. L. Boariu, C. Bareille, H. Schwab, A. Nuber, P. Lejay, T. Durakiewicz, F. Reinert, and A. F. Santander-Syro, Momentum-Resolved Evolution of the Kondo Lattice into "Hidden Order" in URu_2Si_2, Phys. Rev. Lett. **110**, 156404 (2013).

[13] S. Chatterjee, J. Trinckauf, T. Hanke, D. E. Shai, J. W. Harter, T. J. Williams, G. M. Luke, K. M. Shen, and J. Geck, Formation of the Coherent Heavy Fermion Liquid at the Hidden Order Transition in URu_2Si_2, Phys. Rev. Lett. **110**, 186401 (2013).

[14] R. Yoshida, M. Fukui, Y. Haga, E. Yamamoto, Y. Onuki, M. Okawa, W. Malaeb, S. Shin, Y. Muraoka, and T. Yokoya, Observation of two fine structures related to the hidden order in the spectral functions of URu_2Si_2, Phys. Rev. B **85**, 241102(R) (2012).

[15] P. Aynajian, E. Neto, C. V. Parker, Y. Huang, A. Pasupathy, J. Mydosh, and A. Yazdani, Visualizing the formation of the Kondo lattice and the hidden order in URu_2Si_2, Proc. Natl. Acad. Sci. USA **107**, 10383 (2010).

[16] A. R. Schmidt, M. H. Hamidian, P. Wahl, F. Meier, A. V. Balatsky, J. D. Garrett, T. J. Williams, G. M. Luke, and J. C. Davis, Imaging the Fano lattice to 'hidden order' transition in URu_2Si_2, Nature (London) **465**, 570 (2010).

[17] W. K. Park, P. H. Tobash, F. Ronning, E. D. Bauer, J. L. Sarrao, J. D. Thompson, and L. H. Greene, Observation of the Hybridization Gap and Fano Resonance in the Kondo Lattice URu_2Si_2, Phys. Rev. Lett. **108**, 246403 (2012).

[18] J. R. Jeffries, N. P. Butch, B. T. Yukich, and M. B. Maple, The evolution of the ordered states of single-crystal URu_2Si_2 under pressure, J. Phys.: Condens. Matter **20**, 095225 (2008).

[19] E. Hassinger, G. Knebel, T. D. Matsuda, D. Aoki, V. Taufour, and J. Flouquet, Similarity of the Fermi Surface in the Hidden Order State and in the Antiferromagnetic State of URu_2Si_2, Phys. Rev. Lett. **105**, 216409 (2010).

[20] J. R. Jeffries, N. P. Butch, B. T. Yukich, and M. B. Maple, Competing Ordered Phases in URu_2Si_2: Hydrostatic Pressure and Rhenium Substitution, Phys. Rev. Lett. **99**, 217207 (2007).

[21] G. Motoyama, N. Yokoyama, A. Sumiyama, and Y. Oda, Electrical resistivity and thermal expansion measurements of URu_2Si_2 under pressure, J. Phys. Soc. Jpn. **77**, 123710 (2008).

[22] N. P. Butch, J. R. Jeffries, S. Chi, J. B. Leão, J. W. Lynn, and M. B. Maple, Antiferromagnetic critical pressure in URu_2Si_2 under hydrostatic conditions, Phys. Rev. B **82**, 060408(R) (2010).

[23] P. Das, N. Kanchanavatee, J. S. Helton, K. Huang, R. E. Baumbach, E. D. Bauer, B. D. White, V. W. Burnett, M. B. Maple, J. W. Lynn *et al.*, Chemical pressure tuning of URu_2Si_2 via isoelectronic substitution of Ru with Fe, Phys. Rev. B **91**, 085122 (2015).

[24] N. P. Butch, S. Ran, I. Jeon, N. Kanchanavatee, K. Huang, A. Breindel, M. B. Maple, R. L. Stillwell, Y. Zhao, L. Harriger *et al.*, Distinct magnetic spectra in the hidden order and antiferromagnetic phases in $URu_{2-x}Fe_xSi_2$, Phys. Rev. B **94**, 201102(R) (2016).

[25] H. H. Kung, S. Ran, N. Kanchanavatee, V. Krapivin, A. Lee, J. A. Mydosh, K. Haule, M. B. Maple, and G. Blumberg, Analogy Between the "Hidden Order" and the Orbital Antiferromagnetism in $URu_{2-x}Fe_xSi_2$, Phys. Rev. Lett. **117**, 227601 (2016).

[26] M. N. Wilson, T. J. Williams, Y. P. Cai, A. M. Hallas, T. Medina, T. J. Munsie, S. C. Cheung, B. A. Frandsen, L. Liu, Y. J. Uemura *et al.*, Antiferromagnetism and hidden order in isoelectronic doping of URu_2Si_2, Phys. Rev. B **93**, 064402 (2016).

[27] T. J. Williams, A. A. Aczel, and M. B. Stone, Hidden order signatures in the antiferromagnetic phase of $U(Ru_{1-x}Fe_x)_2Si_2$, Phys. Rev. B **95**, 104440 (2017).

[28] C. T. Wolowiec, N. Kanchanavatee, K. Huang, S. Ran, and M. B. Maple, Evolution of critical pressure with increasing Fe substitution in the heavy-fermion system $URu_{2-x}Fe_xSi_2$, Phys. Rev. B **94**, 085145 (2016).

[29] E. Frantzeskakis, J. Dai, C. Bareille, T. C. Rodel, M. Guttler, S. Ran, N. Kanchanavatee, K. Huang, N. Pouse, C. T. Wolowiec *et al.*, From hidden order to antiferromagnetism: Electronic structure changes in Fe-doped URu_2Si_2, Proc. Natl. Acad. Sci. USA **118**, 2020750118 (2021).

[30] S. Zhang, G. Chappell, N. Pouse, R. E. Baumbach, M. B. Maple, L. H. Greene, and W. K. Park, Origin of gaplike behaviors in URu_2Si_2: Combined study via quasiparticle scattering spectroscopy and resistivity measurements, Phys. Rev. B **102**, 081101(R) (2020).

[31] See Supplemental Material at http://link.aps.org/supplemental/10.1103/PhysRevB.106.165109 for XRD measurements of $URu_{2-x}Fe_xSi_2$, transport measurements of $URu_{2-x}Fe_xSi_2$, topographic images and dI/dV spectra taken above different regions or different samples of the U terminations of $URu_{1.85}Fe_{0.15}Si_2$, topographic images and dI/dV spectra taken above different regions or different samples of the Si terminations of $URu_{1.85}Fe_{0.15}Si_2$, and topographic images and dI/dV spectra taken above different regions or different samples of the Si terminations of $URu_{1.85}Fe_{0.15}Si_2$.

[32] S. Ran, C. T. Wolowiec, I. Jeon, N. Pouse, N. Kanchanavatee, B. D. White, K. Huang, D. Martien, T. DaPron, D. Snow *et al.*, Phase diagram and thermal expansion measurements on the system $URu_{2-x}Fe_xSi_2$, Proc. Natl. Acad. Sci. USA **113**, 13348 (2016).

[33] V. Madhavan, W. Chen, T. Jamneala, M. F. Crommie, and N. S. Wingreen, Tunneling into a single magnetic atom: spectroscopic evidence of the Kondo resonance, Science **280**, 567 (1998).

[34] K. Nagaoka, T. Jamneala, M. Grobis, and M. F. Crommie, Temperature Dependence of a Single Kondo Impurity, Phys. Rev. Lett. **88**, 077205 (2002).

[35] C. T. Wolowiec, N. Kanchanavatee, K. Huang, S. Ran, A. J. Breindel, N. Pouse, K. Sasmal, R. E. Baumbach, G. Chappell, P. S. Riseborough *et al.*, Isoelectronic perturbations to f-d-electron hybridization and the enhancement of hidden order in URu_2Si_2, Proc. Natl. Acad. Sci. USA **118**, 2026591118 (2021).

[36] P. Aynajian, E. H. da Silva Neto, A. Gyenis, R. E. Baumbach, J. D. Thompson, Z. Fisk, E. D. Bauer, and A. Yazdani, Visualizing heavy fermions emerging in a quantum critical Kondo lattice, Nature (London) **486**, 201 (2012).

[37] J. H. Shim, K. Haule, and G. Kotliar, Modeling the localized-to-itinerant electronic transition in the heavy fermion system $CeIrIn_5$, Science **318**, 1615 (2007).

[38] M. Maltseva, M. Dzero, and P. Coleman, Electron Cotunneling into a Kondo Lattice, Phys. Rev. Lett. **103**, 206402 (2009).

[39] Q. Y. Chen, D. F. Xu, X. H. Niu, J. Jiang, R. Peng, H. C. Xu, C. H. P. Wen, Z. F. Ding, K. Huang, L. Shu *et al.*, Direct observation of how the heavy-fermion state develops in $CeCoIn_5$, Phys. Rev. B **96**, 045107 (2017).